*Review*

# Advancements in Materials Science and Photocatalysts for Sustainable Development

Dhanalakshmi Vadivel [1,2] , Swetha Suryakumar [3] , Claudio Casella [4] , Andrea Speltini [1] and Daniele Dondi [1,2,*]

1. Department of Chemistry, University of Pavia, Via Taramelli 12, 27100 Pavia, Italy; dhanalakshmi.vadivel@unipv.it (D.V.); andrea.speltini@unipv.it (A.S.)
2. Istituto Nazionale di Fisica Nucleare (INFN), Sezione di Pavia, Via Agostino Bassi 6, 27100 Pavia, Italy
3. Department of Biotechnology, University of Rome-Tor Vergata, Via Cracovia 50, 00133 Rome, Italy; swethajk21@gmail.com
4. Department of Chemical and Environmental Engineering, University of Oviedo, C/Julián Clavería s/n, 33006 Oviedo, Spain; uo285701@uniovi.es
* Correspondence: daniele.dondi@unipv.it

**Abstract:** Materials science and catalysis advancements play a critical role in achieving sustainable development by managing environmental, energy, and resource challenges. Catalyst design advancements focus on enhancing selectivity to achieve sustainable chemical reactions, reducing energy consumption. Designing catalysts that are environmentally friendly and biodegradable is increasingly gaining importance. This aligns with the principles of green chemistry and contributes to minimizing the environmental impact of catalytic processes. These advances, taken as a whole, lead to more sustainable and efficient processes in industries ranging from energy production to pollutant removal, fueling the advancement toward a more sustainable future. Photochemistry, that is, the activation of a stable compound (catalyst) into the highly reactive excited state, is of particular importance, since photons—especially when they come from solar light—are a green and renewable resource. This review article has provided the overall idea of the photocatalysts and materials under green chemistry perspective from the standpoint of the concept of sustainable development.

**Keywords:** catalysts; carbon materials; sustainable energy; $CO_2$ reduction; $H_2$ production; remediation

## 1. Introduction

Water and sunlight are the inexhaustible resources that we have to stabilize our life on Earth and use for the different needs of life, especially for energy. There is an immediate requirement for an energy supply like hydrogen, nicknamed "clean fuel," as it is a fuel with zero carbon dioxide emissions. Being the "energy carrier," hydrogen is considered to be the best alternative to the liquified energy sources used today. According to the U.S. Energy Information Administration (International Energy Outlook, 2021, in Figure 1), by 2050, renewable energy consumption for the generation of electricity will expand by 27%, surpassing the usage of coal and natural gases. It also states that, by 2050, Plug-in Electric Vehicles (PEVs) will grow to make up to one-third of the global light-duty stock. This rate shows a 5% increase in electricity consumption for global transportation by 2050.

In 1972, Fujishima and Honda designed a photo-electrochemical cell that could be used to induce water splitting (or the decomposition of water) for the production of hydrogen gas ($H_2$), using $TiO_2$ as a photocatalyst. The conditions that they put forward to meet the requirement of water splitting or the decomposition of water (for hydrogen production) were that the potential for oxygen evolution is made more negative, and that of hydrogen evolution is made more positive [1].
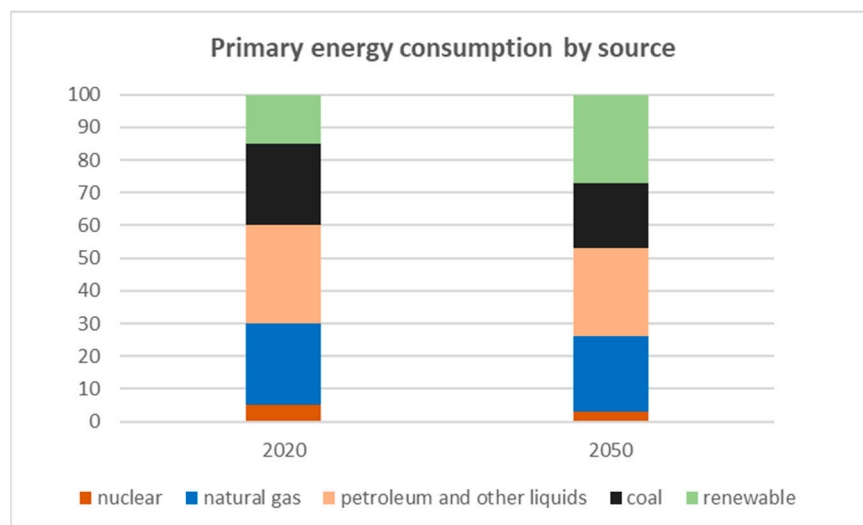
**Figure 1.** International Energy Outlook, 2021.

Photocatalysis occurs when the energy of the incident light is greater than the band gap energy between the conduction band (CB) and the valence band (VB) in a semiconductor material. After the absorption of light, $e^-/h^+$ pairs are generated, as shown in Figure 2. These electron–hole pairs are then transferred to the surface of the photocatalyst, where the splitting of water molecules occurs. The redox potential of the VB should be more positive for the generation of free OH radicals than that of the CB. The major requirements for a semiconductor material to be photochemically active are high stability, sufficient light absorption, favorable band gaps with respect to water oxidation potential, slow recombination rate, and low cost [2]. Photocatalysts are used in a wide range of applications, such as wastewater treatment and hydrogen and freshwater production [3].
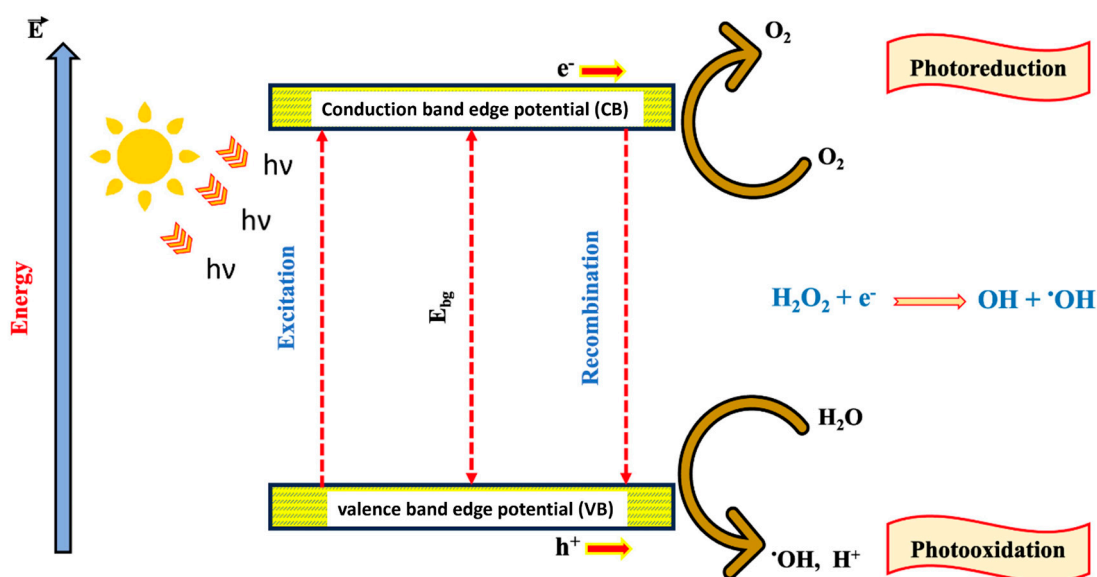


**Figure 2.** Electron–hole pair generation in an illuminated semiconductor particle and consecutive reactions for degradation.

## 2. Photocatalytic Reduction of $CO_2$

Depending on the number of electrons used in the reduction, carbon dioxide reduction can result in a variety of C1 compounds and intermediates. Obviously, transferring a single electron at a time is simple in practice, but single electron reduction of carbon dioxide results in the unstable radical anion intermediate at an extremely high reduction potential.

Nonetheless, the free energy value for the reduction corresponds to a photon in the visible-light spectrum, illustrating the importance of photochemistry [4]. Out of all of the $CO_2$ reduction strategies in this category, photocatalytic methods that use solar energy appear to be the most strategic and in need of improvement, since they have the potential to produce green organic molecules that can be used to produce renewable fuels. Higher levels of catalytic carbon dioxide reduction are limited by inadequate energy efficiency and product selectivity. Rui Pang et al. reported the use of alkaline earth metals to modify the surface of photocatalysts, so as to act as a Lewis base that attracts the acidic $CO_2$. In addition to that, a core–shell Ag@Cr was used as a cocatalyst to help to retain the adsorption of $CO_2$. The composite produced, Ag@Cr/$Ga_2O_3$-Ca, was checked for the photoreduction of $CO_2$ by $H_2O$. It was observed that the photocatalyst Ag@Cr/$Ga_2O_3$-Ca exhibited a high CO formation rate (794.2 $\mu$mol h$^{-1}$) and selectivity to CO absorption at 82%. It was also clear that a significantly lower amount of Ca present on the photocatalyst leads to efficient selectivity of $CO_2$ adsorption on the surface of the catalyst [5].

Shan Hu et al. proposed that strong metal support interactions favor *$CO_2$ adsorption and *COOH generation and desorption by preparing the photocatalyst $Ag_1$@PCN. This photocatalyst was prepared by anchoring Ag single atoms on polygonal $C_3N_4$ nanotubes [6].

Yuxiang Yang conducted a study on nitrogen doping of $In_2O_3$ using discharge-enhanced nitrogen doping via dielectric barrier discharge (DBD) plasma. The resulting N-$In_2O_3$ photocatalyst exhibited enhanced light absorption, superior charge separation efficiency, improved activity, and an increased methanol yield. The controllable production of methanol from $CO_2$ was achieved by tuning the nitrogen doping content. High-resolution transmission electron microscopy (HRTEM) images confirmed the lattice fringes of cubic $In_2O_3$, while elemental mapping showed a uniform distribution of nitrogen on the N-$In_2O_3$ surface. Nitrogen doping altered the charge distribution on the photocatalyst surface. UV–visible diffuse reflectance spectroscopy (UV–Vis–DRS) spectra revealed reduced band gaps for N-$In_2O_3$ variants, enhancing the solar photon collection efficiency [7].

As they are inexpensive and made of earth-abundant and environmentally friendly elements, lead-free magnesium iodide (KMgI3) perovskite films were fabricated by ink-jet printing on different supports, namely glass, mica, and magnesium oxychloride, which work as nucleation sites for the controlled growth of the perovskite. The morphology of the film depended on the type of substrate, with glass favoring the formation of bigger particles and mica inducing agglomerates, while the perovskite cubes trapped in the needle-like morphology were obtained on the latter support. The devices (band gap 3.2–3.4 eV) proved to be capable of generating formic acid by $CO_2$ reduction under visible light, and also $H_2$ gas, with the best performance being shown by the KMgI3 printed on mica, due to more reactive surface being available for the photoreaction and enhanced adhesion of the perovskite to the mica substrate due to the co-sharing of K$^+$ ions. The stability of the photoactive layer, verified over three consecutive photocatalytic cycles, strengthens the sustainability of this lead-free perovskite [8].

The combination of graphitic carbon nitride with inorganic modifiers, proposed for $H_2$ production (see Section 3), has been investigated also to carry forward $CO_2$ reduction in the gas–solid reaction mode. To compensate for indium vanadate ($InVO_4$)'s low reduction capability, short charge carrier lifetime, and poor sorption affinity for $CO_2$, this visible-light active catalyst has been coupled with g-$C_3N_4$ containing nitrogen defects. The latter, obtained by thermal condensation under a $N_2$ atmosphere, was dispersed in a solution with the inorganic precursor, and the composite was finally obtained by hydrothermal treatment. The 30% *w/w* $InVO_4$ composite showed the highest $CO_2$ photoreduction performance under visible illumination, as apparent from the CO, $CH_4$, and formic acid production, which were around two and three times higher compared to the unmodified g-$C_3N_4$ and the inorganic catalyst alone, respectively. The reason of this improvement is the enlarged $CO_2$ adsorption and the enhanced charge carrier separation provided by the formation of a Z-scheme heterojunction between $InVO_4$ and g-$C_3N_4$, wherein the reduction capability

of the latter is powered and conveniently exploited to produce the $CO_2$ byproducts. The stability of the hybrid material, verified by XRD and FT-IR, is reflected in a negligible decrease in efficiency over four irradiations, suggesting a reusability of the catalyst for consecutive photoreactions [9].

Other inorganic co-catalysts can be used to tune the properties of g-$C_3N_4$, as shown by Zhai and co-workers. In their investigation, nickel hydroxide coupled with potassium-doped g-$C_3N_4$ is a working hybrid catalyst for this purpose. The rationale for designing this material comes from the evidence that the incorporation of potassium in the carbon nitride, through calcination, suppresses the electron–hole pairs recombination, and that $Ni(OH)_2$ converts into Ni and NiO during irradiation, working as an electron collector, thus facilitating the reductive reactions and representing a more sustainable approach compared to use of noble (expensive) metals, such as platinum. As highlighted by the transient photocurrent curves, the photocurrent increases in the order of g-$C_3N_4$ < K-g-$C_3N_4$ < 30% $Ni(OH)_2$/K-g-$C_3N_4$, suggesting that the modification of pristine carbon nitride prolongs the electrons' lifetime. Another key point is the enlarged $CO_2$ adsorption rate after coupling with nickel hydroxide and the higher visible-light harvesting compared to use of undoped g-$C_3N_4$, altogether resulting in a boosted carbon dioxide conversion into CO and $CH_4$ (with no decrease in their production over four catalytic cycles), under full spectrum simulated sunlight and just with water as reducing agent [10].

Independently of the specific type of catalyst, the base photoelectronic requirements are the key feature for an efficient $CO_2$ photoreduction process, as discussed by Cheng et al. in the application of the fully conjugated covalent organic framework (COF). Specifically, vinylene-linked COF incorporating rhenium complexes with the bypiridine moieties as reductive sites and triazine ring structures as oxidative sites was prepared by aldol condensation and proved to be efficient for $CO_2$ conversion into CO (around 190 $\mu$mol g$^{-1}$ h$^{-1}$) and simultaneous $O_2$ evolution, under visible light, with no need for sacrificial agents. We can see that combining Re with the conjugated skeleton leads to many advantages, namely (i) an increased sorption affinity for carbon dioxide (+65%); (ii) an efficient charge carrier separation due to a charge transfer channel from ligand to metal, making excited electrons move to the Re complex units to sustain $CO_2$ reduction, while holes in the triazine ring units are consumed for $H_2O$ oxidation; and (iii) a synergistic effect between the base COF and the one embedding the Re complex in terms of $CO_2$ conversion. The cycling stability was verified over five photoreactions and pointed out the substantial stability of the COF, with about 10% decrease in the reaction yield ascribable to Re photobleaching [11].

J.G. Swadener reported the strain engineering of $TiO_2$ shell nanoparticles to obtain the desired band gaps for the photocatalytic activation of $TiO_2$, whose band gap energy is 3.2 eV, limited to the UV range of 375 nm for electron–hole production. A novel $ZrO_2$@$TiO_2$ nanoparticle strain was developed with a $TiO_2$ shell and tetragonal $ZrO_2$ core. A maximum 7% c-axis strain was observed in a 12 nm $ZrO_2$ core and 10 nm $TiO_2$ shell, with a decrease in the band gap of 0.35 eV. The electron–hole generation in this core@shell was predicted to be increased by 22%, with the use of longer wavelength sunlight increasing up to 420 nm. This novel material was predicted to have carbon dioxide reduction photocatalytic activity up to 420 nm, as there was a decreased band gap energy in the shell of $TiO_2$ [12].

Irradiated GO was studied by Yu Kuang et al. for $CO_2$ reduction. The photocatalytic reduction activity of sunlight simulated GO ($G_{ss}$) production, and UV-irradiated GP ($G_{uv}$) was observed to be 2.7- and 2.1-fold higher than that of pristine graphene oxide (GO). $GO_{SS}$ had more CO production than $GO_{UV}$, indicating that simulated sunlight irradiation is better for GO activation [13].

## 3. Photocatalytic Hydrogen Production

The valorization of wastewaters in a circular economy approach to produce clean energy is a smart task and is of great relevance, owing to the possibility to exploit the organic load naturally present in the water effluents and sewage.

Oxidized graphitic carbon nitride (o-g-$C_3N_4$), prepared from a low-cost precursor through a post-synthetic oxidation step—as a photochemically efficient derivative of the pristine carbon nitride, due to the greater surface area and electron-rich states—was compared to commercial Evonik AEROXIDE® P25 $TiO_2$, chosen as the benchmark catalyst, for photocatalytic $H_2$ evolution. To boost the photoreaction, metal co-catalysts were deposited on the catalysts, evaluating Pt or the bimetallic system Cu-Ni, for which a synergistic effect between the two metals was ascertained. It was found that, despite having lower yields than the classical pairing Pt/$TiO_2$, coupling o-g-$C_3N_4$ with Cu-Ni and working with low-cost sacrificial bio-oxygenates (starch and mono- and di-saccharides) in the solution, under simulated solar light, produced significantly higher amounts of $H_2$ compared to pure water, as also verified in untreated sugar-rich wastewaters from the production processes of food industries, such as as dairy and brewery [14].

Another strategy used to boost the performance of g-$C_3N_4$ is the fabrication of heterojunctions with perovskites, possibly avoiding those containing lead. It was reported that the $DMASnBr_3$/g-$C_3N_4$ composite (DMA: dimethylammonium) affords a HER 15-fold higher in aqueous glucose than that found in neat water, with consistent production, also avoiding the use of any metal as a co-catalyst. The synergistic effect between the two constituents of the $DMASnBr_3$-based photocatalyst, which works as a Z-scheme heterojunction, results from favorable band alignment and extended charge carrier lifetimes, in line with the experimental HER that was 12-fold higher than that achieved for the pure carbon nitride. The composite proved to be reusable for three photocatalytic treatments and was able to sustain $H_2$ formation (~150 µmoles $g^{-1}$ $h^{-1}$) when exploiting a raw polysaccharide like soluble starch. With reference to the photoactivity of the heterojunction, this was tested parallel to P25 $TiO_2$ under selected conditions, i.e., with the same catalytic surface area in suspension, gaining 2.5-times higher $H_2$ evolution when using the composite [15].

Z-scheme heterojunction was proposed by Bo et al. using noble elements (carbon quantum dots or CQDs) to obtain effective surface plasmon resonance, band gap width, charge separation, and good visible light utilization. The composite produced was g-$C_3N_4$/$TiO_2$/CQDs/Au nanoparticles, which are shown in Figure 3. The band gap of the composite material was observed to be from 2.9 eV to 3.0 eV, as opposed to the wider band gap width of $TiO_2$. The photocatalytic hydrogen production of the composite was observed to be 6.2 times higher than that of pristine g-$C_3N_4$. This difference was observed owing to the heterojunction formation between g-$C_3N_4$ and $TiO_2$, which helped to reduce the electron–hole pair recombination of pristine g-$C_3N_4$. In addition to that, the introduction of Au nanoparticles and CQDs to the combination enhanced the composite material's ability to absorb visible light [16].
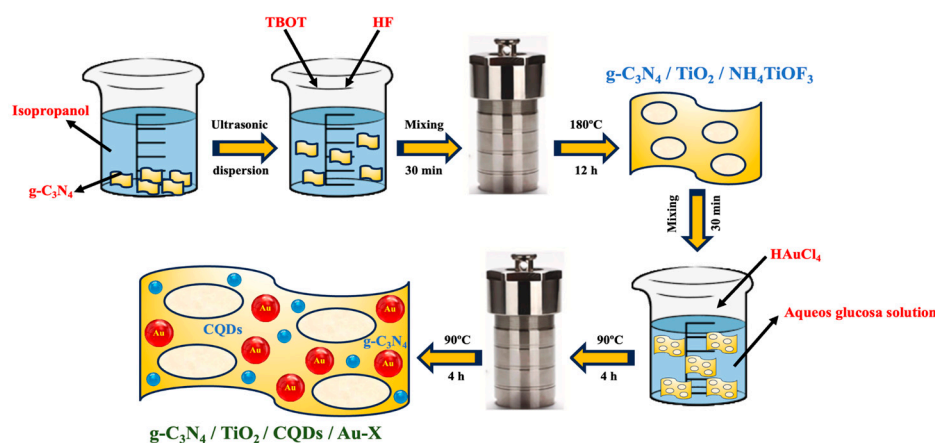


**Figure 3.** Preparation procedure for g-$C_3N_4$/$TiO_2$/CQDs/Au-X.

Kunlei et al. utilized a water-in-oil (*w/o*) microemulsion method to synthesize a core–shell $Cu_xO@TiO_2$ composite material under alkaline conditions. The reasons for

utilizing $Cu_2O$ were its narrow band gap width and its ability to act as a photocatalyst under visible-light irradiation. The material was synthesized with $Cu_2O$ as the core and titania as the shell. A narrow band gap value was seen for the core–shell material, which was probably because of the interfacial charge transfer of the mixed copper oxides. The highest photocatalytic activity for $H_2$ generation was observed with a higher concentration of ground $Cu_XO$. The Z-scheme charge transfer process was confirmed by XPS analysis [17].

A 2D-g-$C_3N_4$/Porphyrin MOF was fabricated by Yuzhi et al., and the hydrogen production capability of the novel nanohybrid was investigated. Characterization studies using SEM imaging showed that the 2D nanohybrid consisted of dispersed sheets, with $\pi$–$\pi$ interaction between porphyrin and g-$C_3N_4$/cobalt ions. The nanohybrid had 15.7-times greater hydrogen generation capacity than the g-$C_3N_4$/cobalt ions without the addition of any co-catalyst. This may be due to the presence of more photoactive sites and a better electron transfer network in the nanohybrid [18].

## 4. Wastewater Treatment

### 4.1. Dye Degradation

Industrial dyeing produces effluents that include organic pollutants that must be treated before being released into natural water sources. Modern approaches to wastewater treatment comprise the implementation of specialized oxidation methodologies, such as photocatalysis, Fenton reactions, and ozonation [19–21].

The photocatalytic activity of a catalyst is often tested by using organic dyes. It is also well known that water polluted with organic dyes is difficult to treat. A combination of physical, chemical, and biological processes is utilized in standard wastewater treatment plants to reduce the amounts of solids and diverse organic and inorganic substances. Aliyar et al. carried out dynamic surface phenomenon analysis to study the interaction between a photocatalyst and the dye for surface dynamics. Malachite green (MG) was used as the target dye, and its surface interaction with $TiO_2$ was determined by drop profile analysis. Their results suggested that a MG-$TiO_2$ nanoparticle complex at pH 9 showcased a decreased mobility of the dye, as compared to the free MG particles, owing to the increased surface tension [22,23].

A novel nanoflower-like CdS/$SnS_2$/$TiO_2$ NTs photocatalyst was synthesized by the hydrothermal method. It was further used for photocatalytic degradation of MB-contaminated water and showed quantitative photodegradation. This material is being suggested as a novel technique for efficient $H_2$ generation, as well as for photocatalytic wastewater treatment [24], which is described in Figure 4.
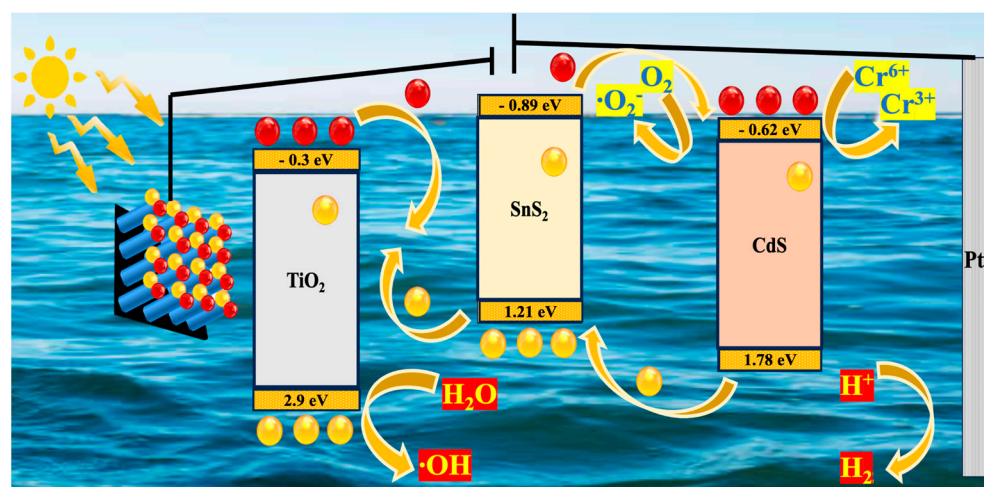


**Figure 4.** Photocatalytic charge carrier transfer mechanism of CdS/$SnS_2$/$TiO_2$ NTs.

Hu et al. [25] designed the "Trash to Treasure" strategy by developing an iodine ($I^-$)-doped hydrothermal carbonation carbon (HTCC), which can be used as a photocatalyst for environmental remediation, as shown in Figure 5.
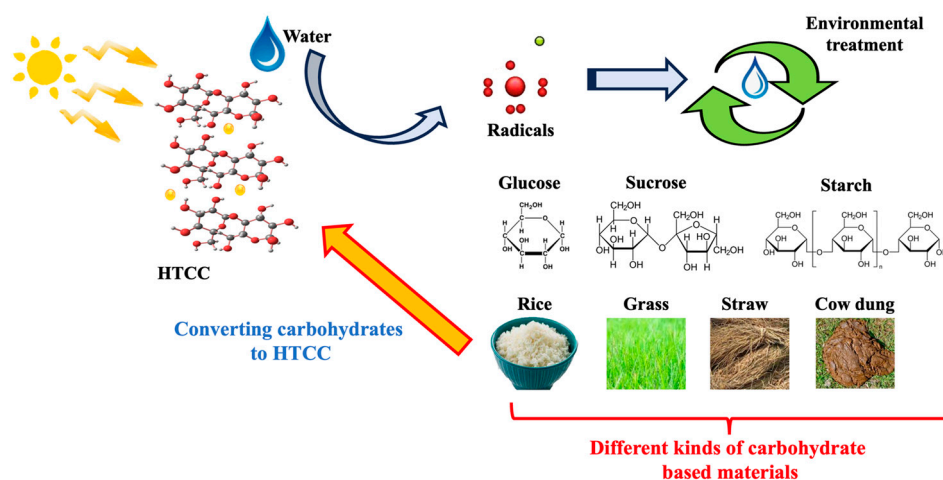


**Figure 5.** Converting carbohydrates into carbon-based photocatalysts for environmental treatment.

The surface area was found to be about 254 m$^2$/g. The characterization studies showed that the iodine-doped HTCC has properties like previously reported polyfuran structures. The Fermi level of I-HTCC was observed in the CB and VB at 0.6 V, 0.26 V, and 1.2 V vs. RHE. The band gap was observed to be 0.94 eV, which was reduced as compared to that of HTCC, which has a band gap of 1.34 eV. It was, therefore, apparent that the band gap narrowed with the insertion of iodine in the HTCC. The generation of OH radicals was observed by a rising peak at 460 nm, as monitored with a coumarin fluorescence probe. The insertion of iodine into the sp$^2$-hybridized polyfuran structure serves as a charge transfer bridge to generate more active hydroxyl radicals, thus increasing the photocatalytic activity [25]. The as-prepared catalyst was checked on the degradation of rhodamine B, and its activity was used for the degradation of organic pollutants and water disinfection.

Salma et al. worked on the green synthesis of a ZnO nanoparticle in combination with *Punica granatum* leaf extract. The characterization studies showed that the green nanoparticles were of an average size of 80 nm. The photolytic activity of the synthesis of the ZnO nanoparticles was tested by photolytic dye degradation of Orange 16 reactive dye. A total of 96% degradation was observed in 30 min in the presence of UV radiation [26].

The ultrasonication approach was used to create layered aluminosilicates of montmorillonite K30 (MK30) with varying ZnO nanoparticle (ZnO NPs) loadings. The photocatalytic degradation process of MB was found to be consistent with the pseudo-first-order kinetic model, with the Zn/MK30 degradation rate constant determined to be $2.86 \times 10^{-2}$ min$^{-1}$. Using *C. edulis* fruit extract, ZnO nanoparticles and a ZnO/MK30 nanocomposite were developed [27].

The photocatalytic degradation study was performed with methyl orange dye under visible-light irradiation, achieving 82% degradation after 150 min of the dye when utilizing less than 20% per mass of catalyst. This corresponds to a three-times-faster degradation rate [28].

Santos et al. made use of Taua (red clay in Brazilian) to form a composite with TiO$_2$, giving rise to a photocatalyst with a narrow band gap. They obtained 80% degradation of MB after 300 min of irradiation in the following conditions: 40 mg/L of MB; 1.7 mg/L of H$_2$O$_2$; pH adjusted to 9, with sodium borate buffer; catalyst 1 mg/mL (6 mL); and irradiation with a high-pressure Hg-Xe arc lamp (Newport) IR, filtered at >418 nm. The band gap energy for the Taua/TiO$_2$ composite was observed to be 2.08 eV, which is equal to anatase Taua, which contains hematite ($\alpha$-Fe$_2$O$_3$). This also coincides with the XRD data that explains the presence of hematite in Taua, and the absorption of the composite

in visible light is due to the presence of hematite. However, the photocatalytic activity of Taua alone is lower (38%) when compared to the composite, which has 100% photocatalytic activity at pH 9 in the presence of hydrogen peroxide. This is attributable to the formation of a heterojunction between $TiO_2$ and $\alpha$-$Fe_2O_3$ and the higher surface area of the composite. $H_2O_2$ enhances the reduction reaction in the following ways [29]:

$$H_2O_2 + e^-(CB) \rightarrow OH\cdot + OH^-$$

$$H_2O_2 + O_2^{\cdot-} \rightarrow OH^- + OH^\cdot + O_2$$
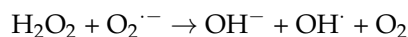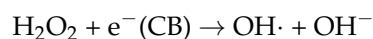
The green synthesis of ultra-small silver nanoparticles was carried out by Sayra et al., using aqueous extracts of *P. hortorum* and *A. fistulosum* as reducing stabilizing agents. The band gap energy for the nanoparticles prepared was 2.38 eV and 2.43 eV, respectively. The ATR-FTIR spectra revealed that the phytochemicals present in the nanoparticles are responsible for reduction-stabilization, as well as capping. The photocatalytic activity of the AgNPs/Phf (from extract of *P. hortorum*) was found to be 95%, and that of AgNPs/Afs (from extract of *A. fistulosum*) was found to be 100% against azo dyes. This high photocatalytic efficiency is due to the narrow band gap energy value. The ultra small size of the synthesized AgNPs/Afs was confirmed to be a mode size of 0.6 nm, with a reported size interval of 0.3 to 0.1 nm, owing to the higher photocatalytic efficiency [30].

A novel core–shell green photocatalyst, $Fe_3O_4$@PDA/CuS, was reported by Ludan et al., with $Fe_3O_4$ as the core–shell, polydopamine (PDA) to be used as a self-polymerizing protectant with the novel semiconductor material, and CuS with a band gap energy of 2.5 eV. The photophysical properties were characterized by UV–Vis DRS, showing that $Fe_3O_4$@PDA had an absorption range in the ultraviolet region, whereas CuS had absorption spectrum in the range of 200–800 nm. The composite $Fe_3O_4$@PDA/CuS demonstrated enhanced absorption in the visible and infrared regions, making it photocatalytically active in natural light. The photocatalyst was seen to have a surface area of about 154 $m^2$/g, with micropore structures determined by the Brunauer–Emmett–Teller test. The photocatalytic activity was tested on an organic probe pollutant like MB, and the degradation was observed to be 92.1% in 180 min under visible light. The magnetic property provided by $Fe_3O_4$ made it possible to easily remove the catalyst from the solution by using a magnet, as it had a magnetic saturation value of 26.01 emu/g (26.01 $Am^2$/kg). The band gap energy of CuS was found to be 2.56 eV [31].

A bi-functional remediation medium was prepared by Amit et al., having both photocatalytic activities provided by bismuth oxychloride (BiOCl) and the absorption activity of biochar produced from kraft lignin, which is shown in Figure 6. The composite was produced by a one-step hydrothermal process. The $S_{BET}$ value showed a surface area of 19 $m^2$/g and 1161 $m^2$/g for BiOCl and biochar, respectively, whereas the $S_{BET}$ value of the composite was 126 $m^2$/g. The biochar was used as a substrate for the synthesis of BiOCl nanoparticles, as seen from the SEM images. The results showed the formation of micro- and mesopores formed by biochar in the composite. This morphological structure allows the diffusion or mass transfer. The band gap energy of BiOCl was initially observed to be 3.43 eV, which, upon the introduction of biochar, dropped down to 3.30 eV. This also led to an increased photocatalytic activity of the composite in the visible-light region, according to the diffuse reflectance spectroscopy (DRS) results.

The microwave-assisted solvothermal method was used by Megxin et al. to synthesize $CuS$@$In_2S_3$-hybridized core–shell nanoparticles. The nanoparticles synthesized by this method took a very short time to form, as compared to other traditional techniques. The photocatalytic activity of the $CuS$@$In_2S_3$-Hy nanoparticles was the highest (MB and MO degradation) at 10% weight, owing to its narrow band gap energy, and the presence of S anions inhibited the recombination of the electron–hole pair formed in the heterojunction [32].
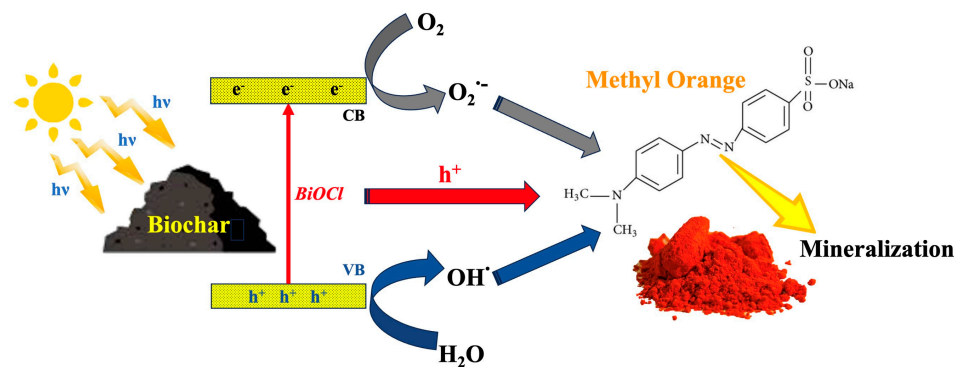
**Figure 6.** Composites of lignin-based biochar with BiOCl for photocatalytic water treatment.

The use of microorganisms as a bio-support material for green photocatalysis is increasingly being studied by scientists. In a study by Akbar et al., *Bacillus thuringiensis* was used to synthesize a nano-biocatalyst coupled with ruthenium/nickel co-doped zinc nanoparticles (btRNZn NPs) to generate hydrogen through the methanolysis of $NaBH_4$. These catalysts are also utilized in the removal of MO dye. The nanoparticles produced were a size of 11.78 nm, as unveiled by TEM analysis. It served as a great biocatalyst, with a photodegradation activity of 68.2% against MO dye after 90 min of irradiation [33].

Diverse graphene-based semiconductor materials with potential as excellent photocatalysts have been discussed [34]. Tamizharasan et al. synthesized sulfur-nitrogen co-doped graphene quantum dots (GQDs) by the top-down approach. Starch was used as the carbon precursor material and thiourea as a precursor material for the S and N elements. The XRD and SEM analyses revealed the morphology of the prepared compound, showing a bulk of graphite with a small amount of amorphous carbon. The concentration of nitrogen, oxygen, and sulfur present in the S,N-GQDs was low in comparison to the carbon element. After the addition of the dopants (S, N) to the GQDs, its band gap energy was observed to decrease from 3.07 eV to 2.54 eV. The dopants acted as photosensitizers, allowing the catalyst to work under visible light, and also slowed down the electron–hole pair recombination. The S,N-GQDs showed high photocatalytic activity against the cationic dye crystal violet (CV) (91% degradation of a 20 ppm solution in 100 min with a 400 W xenon lamp), while the undoped GQDs showed only 56% photodegradation activity in the same conditions. Scavenger studies have demonstrated that three active species were involved in the photocatalytic mechanism, namely $h^+$, $O_2^-$·, and OH [35].

Non-covalently linked composites are unstable in their structure, thus showing a decrease in their photoactivity. This drawback was overcome by Reena et al. by synthesizing a GO/porphyrin composite material with covalent linkages. The solvothermal method was used to prepare the composite with Fe-THPP and GO-COCL. Characterization studies carried out using UV–Vis spectrophotometry highlighted π–π* transition in both GO and Fe-TPP. The photocatalyst was found to have a high specific surface area (68.781 $m^2$/g), providing many catalytically active sites, and the band gap energy value of the nanocomposite was found to be 2.78 eV, according to Tauc's plot. Taking these properties into consideration, the photocatalytic activity of the material was tested against crystal violet dye, and the photodegradation efficiency was found to be 93.45% in 80 min [36].
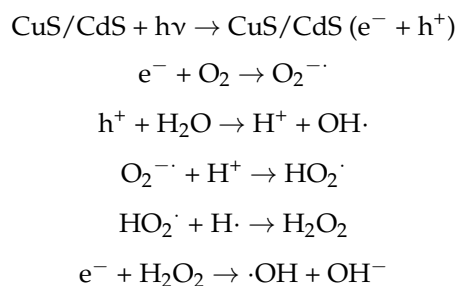
Kraft lignin is often used as a green precursor for activated carbon [37], since its pyrolysis produces different products at different temperatures [38]. The discovery of an extremely persistent peroxyl radical on carbon-modified silica is a significant achievement, because these species are often short-lived. EPR spectroscopy has revealed two distinct forms of peroxyl radicals [39]. The peroxyl radical on carbon-modified silica was exploited by using MB as a reference probe to identify the photocatalytic behavior of the catalyst [40].

### 4.2. Drug Degradation

Drug disintegrating in water is a complicated process that is influenced by multiple variables, including hydrolysis, oxidation [41], photolysis, and microbial metabolism [42]. Understanding the mechanisms and environmental issues associated with drug degradation is essential to formulate efficacious approaches to alleviate pharmaceutical pollution, protect aquatic ecosystems, and maintain public health [43]. "Emerging contaminants" are substances that are present in low concentrations across all ecosystems. In this category of pollutants, there are several medicines, including metoprolol, propranolol, atenolol, and pindolol, among others [37]. They are characteristic compounds of the multi-functionalized aromatic group, are soluble in water, and are susceptible to deionization [44–46].

The photocatalytic degradation of tetracycline-contaminated water bodies by the semiconductor cadmium sulfide nanoparticles along with a co-catalyst, copper sulfide (CuS), was studied by E.V. Sriddharan et al. The CuS/CdS nanocomposite, prepared by a hydrothermal procedure, had the CdS nanorod structure placed over the CuS nanoplate, as revealed by HR-SEM imaging. This structural morphology increased the surface area of the composite and enabled efficient charge separation. CuS/CdS has a band gap energy of 2.30 eV, as calculated from Tauc's plot, with an absorption edge in the visible region at 560 nm, enabling the degradation of tetracycline under sunlight. The results observed in the photoluminescence spectra suggest that the catalyst has a slower electron–hole recombination rate as the intensity of the emission peaks decreases. The composite material exhibited enhanced photocatalytic activity, with a 90% degradation in 50 min under simulated sunlight.

The photocatalytic mechanism of the material was predicted as follows [47]:

$$CuS/CdS + h\nu \rightarrow CuS/CdS\ (e^- + h^+)$$

$$e^- + O_2 \rightarrow O_2^{-\cdot}$$

$$h^+ + H_2O \rightarrow H^+ + OH\cdot$$

$$O_2^{-\cdot} + H^+ \rightarrow HO_2^{\cdot}$$

$$HO_2^{\cdot} + H\cdot \rightarrow H_2O_2$$

$$e^- + H_2O_2 \rightarrow \cdot OH + OH^-$$

Bismuth tungstate has been utilized as a photocatalyst (0.05 g $L^{-1}$) to facilitate the simulated solar light degradation of the antimicrobial ofloxacin (OFL), under relevant real-life conditions (µg $L^{-1}$, freshwater). A quantifiable drug degradation occurred according to a bi-exponential first-order law, with a better efficiency compared to the most commonly employed P25 TiO$_2$ catalyst, as apparent from the higher kinetic constant value (0.38 $min^{-1}$), as experimentally determined. The primary photoproducts analyzed by HPLC-ESI-MS/MS included formerly unidentified photoproducts for this class of pharmaceuticals [48].

Titania can be efficiently layered with pyrolytic carbon by employing a low-cost recyclable resource such as kraft lignin. The crystalline structure of the P25 TiO$_2$ photocatalyst was unaffected by the 600 °C pyrolytic procedure (p-C/TiO$_2$) [49]. The photocatalytic performance of p-C/TiO$_2$ was assessed for the degradation of a fluoroquinolone antimicrobial drug in tap water under simulated sunlight.

2,4-dichlorophenol (2,4-DCP) is a priority contaminant by the Environmental Protection Agency (EPA) from the United States, being an endocrine disruptor with significant bioaccumulation. Its photodegradation conducted by using assessed catalysts like semiconductors is not producing good results, due also to the unknown degradation mechanism. For this particular application, nanostructured NaBiS$_2$ showed an increased efficiency, low toxicity, and antimicrobial effects altogether. Authors have reported an 80% degradation in 18 h of a solution of 50 ppm of 2,4-DCP, with 200 mg/L of catalyst, at pH = 5.3, and under a 50 W LED visible-light source [50].

### 4.3. Other Water Pollutant Removal and Further Applications

Farukh et al. described a method for the synthesis of acidic-group-functionalized catalysts from date pit biomass by in situ carbonization and sulfonation. The activated carbon (ACT-C) and sulfonated carbon (SUL-C) were produced and characterized. XRD studies showed a weak and broad peak between 10° and 40°, similar to the graphite structure. TEM analysis showed the presence of mesopores, in addition to micropores, in SUL-C, due to the sulfonation of the carbon material. After sulfonation, $SO_3H$ occupied a small volume of the pores as the surface area of SUL-C reduced to 272.09 $m^2$/g from 432.4 $m^2$/g in ACT-C. The pore size was also reduced in the SUL-C. TCA analysis exhibited that SUL-C is highly thermally stable, as compared to ACT-C [51].

A ternary composite, $XC/TiO_2/Nb_2O_5$, was created with tannin carbon xerogel incorporated into the $TiO_2/Nb_2O_5$ hybrid photocatalyst. A reduction in crystallite size, along with an increase in surface area, was observed after the addition or incorporation of carbonaceous material to the semiconductor. These morphological changes are predicted to enhance the photocatalytic activity of $TiO_2$. In addition, the incorporation of carbon xerogel exhibited a decrease in band gap energy, thereby allowing the absorption of wavelengths within the visible-light spectrum, i.e., below 380 nm, thereby enhancing the photocatalytic activity by solar light irradiation. The photocatalytic degradation of 4-chlorophenol (4CP) taking place with $XC/TiO_2/Nb_2O_5$ was described as follows [52], as shown in Figure 7.
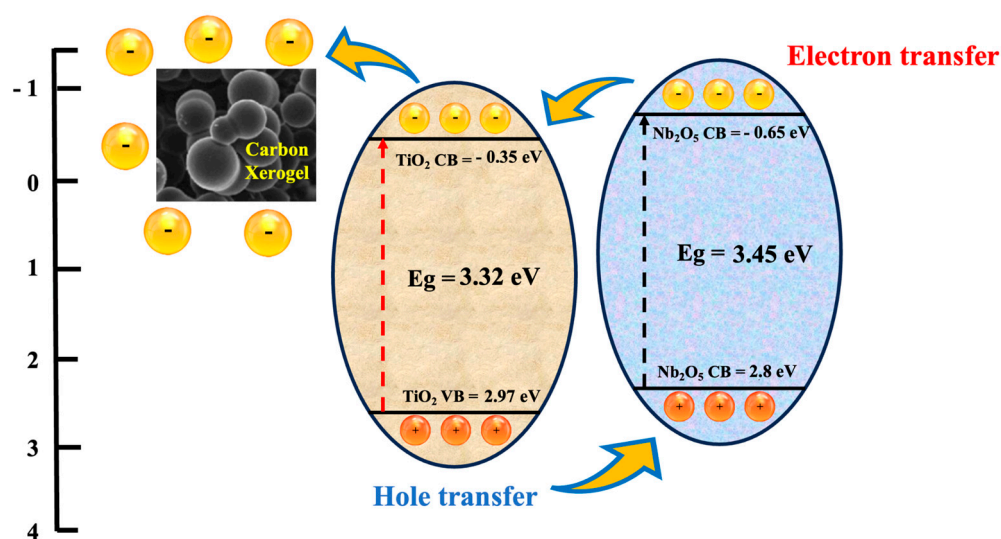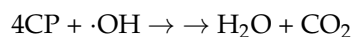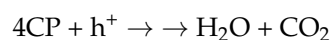


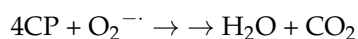**Figure 7.** Band diagram of the $TiO_2/Nb_2O_5$ heterojunction.

$$Photocatalyst + h\nu \rightarrow e^- + h^+$$

$$H_2O + h^+ \rightarrow \cdot OH + H^+$$

$$O_2 + e^- \rightarrow O_2^{-\cdot}$$

$$OH + \cdot OH \rightarrow H_2O_2$$

$$H_2O_2 + e^- \rightarrow \cdot OH + OH^-$$

$$H_2O_2 + O_2^{-\cdot} \rightarrow \cdot OH + O_2 + OH^-$$

$$4CP + O_2^{-\cdot} \rightarrow \rightarrow H_2O + CO_2$$

$$4CP + h^+ \rightarrow \rightarrow H_2O + CO_2$$

$$4CP + \cdot OH \rightarrow \rightarrow H_2O + CO_2$$
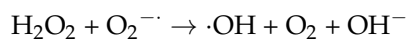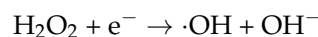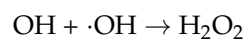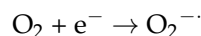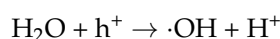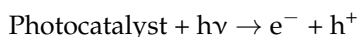
Nicolas et al. published an article describing how kraft-lignin-based carbon xerogel enhanced the photocatalytic activity of ZnO, owing to the morphological changes and an increase in surface area observed in the material after the incorporation of the xerogel. The

material, tested for photocatalytic activity against hexavalent chrome (Cr(VI)) in direct sunlight, demonstrated 20% higher photocatalytic efficiency compared to pure ZnO [53].

The same work was carried forward by the team to synthesize a carbon-based composite utilizing the heterojunctions formed between the semiconductors, viz. carbon semiconductors, and metal semiconductors. This study focused on altering the recombination of charges and improving the photocatalytic activity of ZnO by forming p-n heterojunctions with bismuth oxide and a metallic heterojunction with $Bi^0$ to form hybrid photocatalysts. Lignin/cellulose carbon xerogel functions as a reduction agent of $Bi_2O_3$ and also enhances charge separation. The photocatalytic activity of the composite was tested by the photodegradation of bisphenol-A, providing higher photocatalytic activity in comparison with ZnO/Bi. However, there was no difference in the band gap energy (3.5 eV) in comparison with pure ZnO. The morphological changes observed in XCL/ZnO/Bi were an increase in surface area and pore formation during the addition of the carbon xerogel, as well as the formation of plates and smaller particle aggregates. These characteristics made it possible for the composite to efficiently degrade the dye in the presence of visible light and simulated sunlight [54].

The green synthesis of a novel metal-free photocatalyst, carboxyl-acid-functionalized ionic-liquid-entangled porphyrin photocatalyst (CAFILP) was carried out by Subodh et al. The article focused on the development of a novel photocatalyst to be used for the conversion of sugarcane biorefinery products to value-added compounds. Characterization studies with UV–Vis DRS spectra revealed a band gap energy of 1.49 eV, which allows the photocatalyst to function efficiently in the visible-light range. The synthesized photocatalyst has a relative acidity of 0.99 (as shown by the Hammett value), and the material is predicted to have substantial proton levels. Thereby, the photocatalyst is seen to have more acid sites to form bonds with the substrate. Molasses was used as the substrate for conversion to ethyl levulinate by the action of a photocatalyst under a 5 W LED light. The highest conversion rate was observed after 25 h with 18 mg of photocatalyst (about 1% $m/m$), with a yield of 94% in the presence of ethanol [55].

This study continued to use the novel photocatalyst for the esterification of levulinic acid and the etherification of biomass-derived glycerol. The best conditions for catalytic action were 1% m/m of the photocatalyst for an 18 h reaction time to obtain 78% levulinates from the biomass converted to levulinic acid. The etherification of glycerol was seen to obtain a yield of 88% under optimal photocatalytic conditions [56].

A graphene oxide/porphyrin nanocomposite was prepared via non-covalent interactions, employing two forms of porphyrin, i.e., tetraphenylporphyrin (TPP) and zinc tetraphenylporphyrin (ZnTPP). The UV–Visible absorption spectra of the composite showed a shift in wavelength, reflecting the $\pi$–$\pi$ interaction of the porphyrins with the GO $sp^2$ carbons. It was also apparent that GO was able to form a more stable complex with ZnTPP than TPP, because of the interaction with the oxygen in the ZnTPP core. The photocatalytic activity of the nanocomposite was studied in terms of the oxidation of benzyl alcohol under visible-light irradiation. It was observed that GO-TPP had higher catalytic activity than ZnTPP, probably due to the presence of more active sites of graphene on GO-TPP than on its counterpart. As discussed in earlier sections, epoxides of GO and the Zn center of ZnTPP hindered the active sites for the GO-catalyzed oxidation of alcohols. TPP aggregation on the GO surface, on the other hand, exposed some sections of the GO surface, exposing the accessible active sites [57].

A green method for uranium recovery from water by the production of photosynthetic $H_2O_2$ was proposed by Lang et al. The photocatalyst used was prepared by an aldimine reaction between 5,10,15,20-(tetra-4-aminophenyl)porphyrin-Ni (TPP-Ni) and thieno[3,2-b]thiophene-2,5-dicarbaldehyde (TT) to produce the TT-Por/covalent organic framework (COF)-Ni. The photocatalyst enables the synthesis of $H_2O_2$ without any co-catalyst or sacrificial agent, with the subsequent recovery of (metastudtite) uranium. The band gap energy of the synthesized photocatalyst was 2.01 eV and the VB and CB values were feasible

for the oxygen reduction reaction (ORR), allowing the synthesis of hydrogen peroxide. The photocatalytic removal of uranium was noted to be 94% under solar light [56].

## 5. Conclusions

Visible-light photocatalysis, especially when the catalyst is prepared from renewable resources [58] or microorganisms, can be considered as sustainable [59]. The possibility of photocatalysis spans from wastewater treatment to carbon dioxide reduction and hydrogen production, some of the hottest topics nowadays. In modern chemistry, the use of nanomaterials, especially when noble metals (or toxic metals) are employed, should be reconsidered. In fact, carbon materials are attracting more and more attention, especially when they are derived from natural resources (like graphite and its derivatives) or produced by pyrolysis from biomasses. The ability of carbon to create from zero- to three-dimensional structures, together with the possibility of 'doping' by the addition of other materials, is unrivalled, and only nowadays we are starting to explore and understand their properties. In fact, carbon materials could act as photocatalysts by themselves or in conjunction with other inorganic materials. Furthermore, porous carbon materials have a high capacity of absorbing chemicals. This can be implemented both in water treatment for the removal of pollutants and in soils as biochar.

## References

1. Fujishima, A.; Honda, K. Electrochemical Photolysis of Water at a Semiconductor Electrode. *Nature* **1972**, *238*, 37–38. [CrossRef]
2. Photocatalysis: Present, Past and Future. In *Materials Research Foundations*; Materials Research Forum LLC: Millersville, PA, USA, 2018; Volume 29, pp. 183–206. ISBN 978-1-945291-63-0.
3. Demir, M.E.; Dincer, I. An Integrated Solar Energy, Wastewater Treatment and Desalination Plant for Hydrogen and Freshwater Production. *Energy Convers. Manag.* **2022**, *267*, 115894. [CrossRef]
4. Vadivel, D.; Ferraro, F.; Merli, D.; Dondi, D. Carbon Dioxide Photoreduction in Prebiotic Environments. *Photochem. Photobiol. Sci.* **2022**, *21*, 863–878. [CrossRef]
5. Pang, R.; Teramura, K.; Morishita, M.; Asakura, H.; Hosokawa, S.; Tanaka, T. Enhanced CO Evolution for Photocatalytic Conversion of $CO_2$ by $H_2O$ over Ca Modified $Ga_2O_3$. *Commun. Chem.* **2020**, *3*, 137. [CrossRef]
6. Hu, S.; Qiao, P.; Yi, X.; Lei, Y.; Hu, H.; Ye, J.; Wang, D. Selective Photocatalytic Reduction of $CO_2$ to CO Mediated by Silver Single Atoms Anchored on Tubular Carbon Nitride. *Angew. Chem.* **2023**, *135*, e202304585. [CrossRef]
7. Yang, Y.; Pan, Y.-X.; Tu, X.; Liu, C. Nitrogen Doping of Indium Oxide for Enhanced Photocatalytic Reduction of $CO_2$ to Methanol. *Nano Energy* **2022**, *101*, 107613. [CrossRef]
8. Luévano-Hipólito, E.; Fabela-Cedillo, M.G.; Torres-Martínez, L.M. Novel Lead-Free Halide Perovskite $KMgI_3$ for Photocatalytic Hydrogen Evolution (HER) and Carbon Dioxide Reduction Reaction ($CO_2$RR). *Mater. Lett.* **2024**, *361*, 136066. [CrossRef]
9. Yu, M.; Wang, J.; Li, G.; Zhang, S.; Zhong, Q. Construction of 3D/2D Indium Vanadate/Graphite Carbon Nitride with Nitrogen Defects Z-Scheme Heterojunction for Improving Photocatalytic Carbon Dioxide Reduction. *J. Mater. Sci. Technol.* **2023**, *154*, 129–139. [CrossRef]
10. Zhai, M.; Zhang, Y.; Xu, J.; Lin, H.; Wang, J.; Wang, L. Nickel Hydroxide-Decorating Potassium-Doped Graphitic Carbon Nitride for Boosting Photocatalytic Carbon Dioxide Reduction. *J. Colloid Interface Sci.* **2023**, *650*, 1671–1678. [CrossRef]
11. Cheng, Y.; Ji, W.; Hao, P.; Qi, X.; Wu, X.; Dou, X.; Bian, X.; Jiang, D.; Li, F.; Liu, X.; et al. A Fully Conjugated Covalent Organic Framework with Oxidative and Reductive Sites for Photocatalytic Carbon Dioxide Reduction with Water. *Angew. Chem. Int. Ed.* **2023**, *62*, e202308523. [CrossRef]

12. Swadener, J.G. Strain Engineering of ZrO$_2$@TiO$_2$ Core@shell Nanoparticle Photocatalysts. *Solar* **2023**, *3*, 15–24. [CrossRef]
13. Kuang, Y.; Shang, J.; Zhu, T. Photoactivated Graphene Oxide to Enhance Photocatalytic Reduction of CO$_2$. *ACS Appl. Mater. Interfaces* **2020**, *12*, 3580–3591. [CrossRef] [PubMed]
14. Speltini, A.; Gualco, F.; Maraschi, F.; Sturini, M.; Dondi, D.; Malavasi, L.; Profumo, A. Photocatalytic Hydrogen Evolution Assisted by Aqueous (Waste)Biomass under Simulated Solar Light: Oxidized g-C$_3$N$_4$ vs. P25 Titanium Dioxide. *Int. J. Hydrogen Energy* **2019**, *44*, 4072–4078. [CrossRef]
15. Speltini, A.; Romani, L.; Dondi, D.; Malavasi, L.; Profumo, A. Carbon Nitride-Perovskite Composites: Evaluation and Optimization of Photocatalytic Hydrogen Evolution in Saccharides Aqueous Solution. *Catalysts* **2020**, *10*, 1259. [CrossRef]
16. Lv, B.; Feng, X.; Lu, L.; Xia, L.; Yang, Y.; Wang, X.; Zou, X.; Wang, H.; Zhang, F. Facile Synthesis of G-C$_3$N$_4$/TiO$_2$/CQDs/Au Z-Scheme Heterojunction Composites for Solar-Driven Efficient Photocatalytic Hydrogen. *Diam. Relat. Mater.* **2021**, *111*, 108212. [CrossRef]
17. Wang, K.; Bielan, Z.; Endo-Kimura, M.; Janczarek, M.; Zhang, D.; Kowalski, D.; Zielińska-Jurek, A.; Markowska-Szczupak, A.; Ohtani, B.; Kowalska, E. On the Mechanism of Photocatalytic Reactions on Cu$_x$O@TiO$_2$ Core–Shell Photocatalysts. *J. Mater. Chem. A* **2021**, *9*, 10135–10145. [CrossRef]
18. Zhou, Y.; Zhang, T.; Zhu, W.; Qin, L.; Kang, S.-Z.; Li, X. Enhanced Light Absorption and Electron Transfer in Dimensionally Matched Carbon Nitride/Porphyrin Nanohybrids for Photocatalytic Hydrogen Production. *Fuel* **2023**, *338*, 127394. [CrossRef]
19. Chen, S.; Ren, T.; Zhou, Z.; Lu, K.; Huang, X.; Zhang, X. Insights into Mn Loaded Carbon-Silica-Membrane Based Catalytic Ozonation Process for Efficient Wastewater Treatment: Performance and Mechanism. *Chem. Eng. J.* **2023**, *475*, 145874. [CrossRef]
20. Lee, K.-T.; Ho, K.-Y.; Chen, W.-H.; Kwon, E.E.; Lin, K.-Y.A.; Liou, S.-R. Construction and Demolition Waste as a High-Efficiency Advanced Process for Organic Pollutant Degradation in Fenton-like Reaction to Approach Circular Economy. *Environ. Pollut.* **2023**, *335*, 122246. [CrossRef]
21. Sarvothaman, V.P.; Velisoju, V.K.; Subburaj, J.; Panithasan, M.S.; Kulkarni, S.R.; Castaño, P.; Turner, J.; Guida, P.; Roberts, W.L.; Nagarajan, S. Is Cavitation a Truly Sensible Choice for Intensifying Photocatalytic Oxidation Processes?—Implications on Phenol Degradation Using ZnO Photocatalysts. *Ultrason. Sonochem.* **2023**, *99*, 106548. [CrossRef]
22. Javadi, A.; Nourizade, M.; Rahmani, M.; Eckert, K. Interaction of Catalyst Nanoparticles and Pollutant Molecules in Photocatalytic Wastewater Treatment: Novel Characterization via Dynamic Surface Properties. *Chem. Eng. Sci.* **2023**, *269*, 118459. [CrossRef]
23. Sonune, A.; Ghate, R. Developments in Wastewater Treatment Methods. *Desalination* **2004**, *167*, 55–63. [CrossRef]
24. Zhu, S.; Wu, G.; Liu, Z.; Zhao, S.; Cao, D.; Li, C.; Liu, G. Nanoflower-like CdS and SnS$_2$ Loaded TiO$_2$ Nanotube Arrays for Photocatalytic Wastewater Treatment and Hydrogen Production. *Ceram. Int.* **2023**, *49*, 5893–5904. [CrossRef]
25. Hu, Z.; Shen, Z.; Yu, J.C. Converting Carbohydrates to Carbon-Based Photocatalysts for Environmental Treatment. *Environ. Sci. Technol.* **2017**, *51*, 7076–7083. [CrossRef] [PubMed]
26. Al-Zahrani, S.A.; Patil, M.B.; Mathad, S.N.; Patil, A.Y.; Otaibi, A.A.; Masood, N.; Mansour, D.; Khan, A.; Manikandan, A.; Syafri, E. Photocatalytic Degradation of Textile Orange 16 Reactive Dye by ZnO Nanoparticles Synthesized via Green Route Using Punica Granatum Leaf Extract. *Crystals* **2023**, *13*, 172. [CrossRef]
27. Chellapandi, T.; Madhumitha, G.; Roopan, S.M.; Elamathi, M.; Leeladevi, K.; Nagarajan, E.R.; Vadivel, D.; Dondi, D. Construction of ZnO Nanoparticles on the Layered Aluminosilicate Montmorillonite K30 Nanocomposite and Its Enhanced Photocatalytic Removal Performance. *Opt. Mater.* **2023**, *142*, 114099. [CrossRef]
28. Singh, A.; Giannakoudakis, D.; Arkas, M.; Triantafyllidis, K.; Nair, V. Composites of Lignin-Based Biochar with BiOCl for Photocatalytic Water Treatment: RSM Studies for Process Optimization. *Nanomaterials* **2023**, *13*, 735. [CrossRef] [PubMed]
29. Santos, L.R.D.; Mascarenhas, A.J.S.; Silva, L.A. Preparation and Evaluation of Composite with a Natural Red Clay and TiO$_2$ for Dye Discoloration Assisted by Visible Light. *Appl. Clay Sci.* **2017**, *135*, 603–610. [CrossRef]
30. Bustos-Guadarrama, S.; Nieto-Maldonado, A.; Flores-López, L.Z.; Espinoza-Gomez, H.; Alonso-Nuñez, G. Photocatalytic Degradation of Azo Dyes by Ultra-Small Green Synthesized Silver Nanoparticles. *J. Taiwan Inst. Chem. Eng.* **2023**, *142*, 104663. [CrossRef]
31. Shang, L.; Li, W.; Wang, X.; Ma, L.; Li, L.; Duan, Q.; Li, Y. Preparation of Magnetic Fe$_3$O$_4$@PDA/CuS Core-Shell Nanocomposite as a Green Photocatalyst. *Synth. Met.* **2023**, *292*, 117230. [CrossRef]
32. Liu, M.; Sheardy, A.; Pathiraja, G.; Tukur, F.; Jayapalan, A.; Wei, J. Tuning the Core-Shell Ratio in Nanostructured CuS@In$_2$S$_3$ Photocatalyst for Efficient Dye Degradation. *Clean. Chem. Eng.* **2023**, *5*, 100093. [CrossRef]
33. Hojjati-Najafabadi, A.; Aygun, A.; Tiri, R.N.E.; Gulbagca, F.; Lounissaa, M.I.; Feng, P.; Karimi, F.; Sen, F. *Bacillus Thuringiensis* Based Ruthenium/Nickel Co-Doped Zinc as a Green Nanocatalyst: Enhanced Photocatalytic Activity, Mechanism, and Efficient H$_2$ Production from Sodium Borohydride Methanolysis. *Ind. Eng. Chem. Res.* **2023**, *62*, 4655–4664. [CrossRef]
34. Pastrana-Martínez, L.M.; Morales-Torres, S.; Figueiredo, J.L.; Faria, J.L.; Silva, A.M.T. Graphene Photocatalysts. In *Multifunctional Photocatalytic Materials for Energy*; Elsevier: Amsterdam, The Netherlands, 2018; pp. 79–101. ISBN 978-0-08-101977-1.
35. Selvakumar, T.; Rajaram, M.; Natarajan, A.; Harikrishnan, L.; Alwar, K.; Rajaram, A. Highly Efficient Sulfur and Nitrogen Codoped Graphene Quantum Dots as a Metal-Free Green Photocatalyst for Photocatalysis and Fluorescent Ink Applications. *ACS Omega* **2022**, *7*, 12825–12834. [CrossRef] [PubMed]
36. Raveena; Singh, M.P.; Sengar, M.; Kumari, P. Synthesis of Graphene Oxide/Porphyrin Nanocomposite for Photocatalytic Degradation of Crystal Violet Dye. *ChemistrySelect* **2023**, *8*, e202203272. [CrossRef]

37. Speltini, A.; Sturini, M.; Maraschi, F.; Mandelli, E.; Vadivel, D.; Dondi, D.; Profumo, A. Preparation of Silica-Supported Carbon by Kraft Lignin Pyrolysis, and Its Use in Solid-Phase Extraction of Fluoroquinolones from Environmental Waters. *Microchim. Acta* **2016**, *183*, 2241–2249. [CrossRef]

38. Dondi, D.; Zeffiro, A.; Speltini, A.; Tomasi, C.; Vadivel, D.; Buttafava, A. The Role of Inorganic Sulfur Compounds in the Pyrolysis of Kraft Lignin. *J. Anal. Appl. Pyrolysis* **2014**, *107*, 53–58. [CrossRef]

39. Vadivel, D.; Speltini, A.; Zeffiro, A.; Bellani, V.; Pezzini, S.; Buttafava, A.; Dondi, D. Reactive Carbons from Kraft Lignin Pyrolysis: Stabilization of Peroxyl Radicals at Carbon/Silica Interface. *J. Anal. Appl. Pyrolysis* **2017**, *128*, 346–352. [CrossRef]

40. Vadivel, D.; Malaichamy, I. Pyrolytic formation and photoactivity of reactive oxygen species in a $SiO_2$/carbon nanocomposite from kraft lignin. *F1000Research* **2018**, *7*, 1574. [CrossRef] [PubMed]

41. Mohamadpour, F.; Mohamadpour, F. Photodegradation of Six Selected Antipsychiatric Drugs; Carbamazepine, Sertraline, Amisulpride, Amitriptyline, Diazepam, and Alprazolam in Environment: Efficiency, Pathway, and Mechanism—A Review. *Sustain. Environ. Res.* **2024**, *34*, 8. [CrossRef]

42. Tang, G.; Chen, Y.; Lin, S.; Li, X. The Photo- and Microbial Degradation Kinetics and Pathways of Sulfadoxine in Seawater Elucidated by Liquid Chromatography Coupled with Time-of-Flight Mass Spectrometry. *Chemosphere* **2024**, *351*, 141225. [CrossRef]

43. Renu; Kaur, J.; Garg, T.; Aggarwal, D.; Kumar, V.; Tikoo, K.; Kaushik, A.; Singhal, S. Synthesis of Novel $\alpha$-Cyclodextrin Conjugated $ZnFe_2O_4$-GO Nanocomposites for Electrochemical Detection of Hazardous Imidacloprid Insecticide and Enhanced Photodegradation of Levofloxacin Drug. *J. Electroanal. Chem.* **2024**, *956*, 118074. [CrossRef]

44. Zhang, R.; Zhang, G.; Zheng, Q.; Tang, J.; Chen, Y.; Xu, W.; Zou, Y.; Chen, X. Occurrence and Risks of Antibiotics in the Laizhou Bay, China: Impacts of River Discharge. *Ecotoxicol. Environ. Saf.* **2012**, *80*, 208–215. [CrossRef] [PubMed]

45. Zou, S.; Xu, W.; Zhang, R.; Tang, J.; Chen, Y.; Zhang, G. Occurrence and Distribution of Antibiotics in Coastal Water of the Bohai Bay, China: Impacts of River Discharge and Aquaculture Activities. *Environ. Pollut.* **2011**, *159*, 2913–2920. [CrossRef] [PubMed]

46. Martínez Bueno, M.J.; Hernando, M.D.; Agüera, A.; Fernández-Alba, A.R. Application of Passive Sampling Devices for Screening of Micro-Pollutants in Marine Aquaculture Using LC–MS/MS. *Talanta* **2009**, *77*, 1518–1527. [CrossRef] [PubMed]

47. Siddhardhan, E.V.; Surender, S.; Arumanayagam, T. Degradation of Tetracycline Drug in Aquatic Environment by Visible Light Active CuS/CdS Photocatalyst. *Inorg. Chem. Commun.* **2023**, *147*, 110244. [CrossRef]

48. Vadivel, D.; Sturini, M.; Speltini, A.; Dondi, D. Tungsten Catalysts for Visible Light Driven Ofloxacin Photocatalytic Degradation and Hydrogen Production. *Catalysts* **2022**, *12*, 310. [CrossRef]

49. Vadivel, D.; Branciforti, D.S.; Speltini, A.; Sturini, M.; Bellani, V.; Malaichamy, I.; Dondi, D. Pyrolytic Formation of $TiO_2$/Carbon Nanocomposite from Kraft Lignin: Characterization and Photoactivities. *Catalysts* **2020**, *10*, 270. [CrossRef]

50. Kumar, V.D.; Balaji, K.R.; Viswanatha, R.; Ambika, G.; Roopa, R.; Basavaraja, B.M.; Santosh, M.S. Visible light photodegradation of 2, 4-dichlorophenol using nanostructured $NaBiS_2$: Kinetics, cytotoxicity, antimicrobial and electrochemical studies of the photocatalyst. *Chemosphere* **2022**, *287*, 132174. [CrossRef] [PubMed]

51. Jamil, F.; Al-Muhtaseb, A.H.; Naushad, M.; Baawain, M.; Al-Mamun, A.; Saxena, S.K.; Viswanadham, N. Evaluation of Synthesized Green Carbon Catalyst from Waste Date Pits for Tertiary Butylation of Phenol. *Arab. J. Chem.* **2020**, *13*, 298–307. [CrossRef]

52. De Moraes, N.P.; Torezin, F.A.; Jucá Dantas, G.V.; De Sousa, J.G.M.; Valim, R.B.; Da Silva Rocha, R.; Landers, R.; Da Silva, M.L.C.P.; Rodrigues, L.A. $TiO_2$/$Nb_2O_5$/Carbon Xerogel Ternary Photocatalyst for Efficient Degradation of 4-Chlorophenol under Solar Light Irradiation. *Ceram. Int.* **2020**, *46*, 14505–14515. [CrossRef]

53. De Moraes, N.P.; De Siervo, A.; Silva, T.O.; Da Silva Rocha, R.; Reddy, D.A.; Lianqing, Y.; De Vasconcelos Lanza, M.R.; Rodrigues, L.A. Kraft Lignin-Based Carbon Xerogel/Zinc Oxide Composite for 4-Chlorophenol Solar-Light Photocatalytic Degradation: Effect of pH, Salinity, and Simultaneous Cr(VI) Reduction. *Environ. Sci. Pollut. Res.* **2023**, *30*, 8280–8296. [CrossRef] [PubMed]

54. De Moraes, N.P.; Campos, T.M.B.; Thim, G.P.; De Siervo, A.; Lanza, M.R.D.V.; Rodrigues, L.A. Application of a New Lignin/Cellulose Carbon Xerogel/ZnO/$Bi_2O_3$/Bi° Composite Photocatalyst for the Degradation of Bisphenol-A under Sunlight. *Chem. Phys. Impact* **2023**, *6*, 100182. [CrossRef]

55. Raut, S.U.; Bhagat, P.R. Sugarcane Bio-Refinery Products: An Efficient One Umbrella Approach for Synthesis of Biofuel and Value-Added Compounds Using Metal-Free Photo-Catalyst. *Fuel* **2021**, *303*, 121154. [CrossRef]

56. Chen, L.; Hang, J.; Chen, B.; Kang, J.; Yan, Z.; Wang, Z.; Zhang, Y.; Chen, S.; Wang, Y.; Jin, Y.; et al. Photocatalytic Uranium Removal from Basic Effluent by Porphyrin-Ni COF as the Photocatalyst. *Chem. Eng. J.* **2023**, *454*, 140378. [CrossRef]

57. Phuangburee, T.; Solonenko, D.; Plainpan, N.; Thamyongkit, P.; Zahn, D.R.T.; Unarunotai, S.; Tuntulani, T.; Leeladee, P. Surface Modification of Graphene Oxide *via* Noncovalent Functionalization with Porphyrins for Selective Photocatalytic Oxidation of Alcohols. *New J. Chem.* **2020**, *44*, 8264–8272. [CrossRef]

58. Dondi, D.; Vadivel, D. Preparation of catalysts from renewable and waste materials. *Catalysts* **2020**, *10*, 662. [CrossRef]

59. Ravelli, D.; Dondi, D.; Fagnoni, M.; Albini, A. Photocatalysis. A multi-faceted concept for green chemistry. *Chem. Soc. Rev.* **2009**, *38*, 1999–2011. [CrossRef]